Performance of dynamic decoupling control sequences on trapped $^{40}Ca^{+}$

By Kenneth Wright

Submitted to the
School of Chemistry and Biochemistry
in partial fulfillment of the
requirements for the degree
Bachelor of Science in Chemistry

GEORGIA INSTITUTE OF TECHNOLOGY
May 2010

Table of Contents

Table of Figures

Chapter I

1.1 Introduction

One of the fundamental problems of chemistry is the difficulty in determining full quantum mechanical descriptions of molecules. Molecules contain many degrees of freedom and as a result the classical description scales factorially with the number of electrons. One way to overcome this mismatch between quantum and classical pictures is to use one quantum system, a quantum computer, to simulate another. Quantum computation is based upon a two-level system, a qubit, which is analogous to a bit in classical computation. Unlike a classical bit, a qubit can exist in a superposition of quantum states. The interaction between a quantum system and its environment results in the decay of the superposition state of the system into a probability density of classical states [1]. This is known as decoherence.

A realistic quantum computer requires qubits with long coherence times; with respect to the achievable gating times, for a formal relation refer to section 1.2.2. The spin echo effect in nuclear magnetic resonance (NMR) offers a way to increase the coherence time of a qubit and has been studied as a way to mitigate decoherence in quantum computation[2][3]. By applying an appropriate π pulse to a system under the influence of a large external field, as in NMR, the interaction term of the Hamiltonian between the qubit and environment can be eliminated[3][4]. Periodic implementation of such pulses is known as periodic dynamic decoupling (PDD). Similar to PDD, concatenated dynamic decoupling (CDD) is a periodic pulse sequence which removes the interaction term of the Hamiltonian, however in CDD pulse sequences are recursively embedded within the overall pulse train. Such pulse sequences have been shown theoretically to work for model quantum systems such as GaAs quantum dots, and theoretically such pulse sequences vastly improve the coherence time of a qubit [5]. There have been many calculations showing that by progressively increasing the number of concatenated pulse sequences increasingly longer coherence times can be achieved [6][7]. These techniques have not been tested in the laboratory and experimental implementation of these promising techniques motivates current research. There also continues to be extensive work on developing novel pulse sequences which may improve coherence times even further. The goal of this research is to experimentally determine the coherence times which can be achieved with a trapped calcium atom by applying these pulse sequences.

1.2 Background

There are many possible qubit systems which are being researched, one of the most promising are trapped ions. Trapped ions have the advantage of few mechanisms for decoherence and also interact strongly with electromagnetic fields. Pulse sequences have been shown to significantly increase the coherent control of trapped ions. The only experimental implementation of coherence control with trapped ions was done using the Uhrig dynamic decoupling (UDD) pulse sequence. This is an optimization of the Carr-Purcell-Meiboom-Gill (CPMG) pulse sequence, which was developed by the NMR community [4]. The optimization is in the delay between applied π pulses. It has been shown theoretically and experimentally that a UDD type pulse sequence is superior in preventing decoherence than the CPMG pulse scheme devised in the 1950's [8]. There has been no successful experimental implementation of a concatenated dynamic decoupling (CDD) pulse sequence or any other dynamic decoupling sequence on trapped ions.

1.2.1 Ion Traps

Ion traps were developed in the 1970's and have become a popular experimental system to develop technologies used for optical clocks and to perform high resolution spectroscopy [9]. To discuss dynamic decoupling using a trapped calcium ion, It is necessary to discuss some of the fundamentals of ion trapping and how trapped ions interact with radiation [10].

Ion traps take advantage of the strong electrodynamic forces which act upon an ion to constrain its motion to a given region of space. This is accomplished by creating a gradient field (electric or magnetic) with a geometry which constrains the motion of the ion in all directions. For an electrostatic potential this violates Laplace's equation, there can be no local minima or maxima within a given electric field, all extrema must occur at the boundary of the surface. This difficulty can be overcome by creating a time varying electric field which quickly oscillates between fields that constrain the motion in different directions [9][12].

Laplace's Equation (Eq. 1)

$$\nabla^2 V = 0$$

In two dimension (Eq. 2)

$$\frac{\partial^2 V}{\partial x^2} + \frac{\partial^2 V}{\partial z^2} = 0 \text{ [12]}$$

To maximize the force on the ion from the potential, a saddle point is the best surface that and still satisfies Laplace's equation. By quickly varying the high and low potential regions, the ion is confined at the base of the saddle. In this region of low potential the ion will be trapped if the switching between high and low potentials is quick with respect to the ion motion. If this is the case the ion will view the pseudo-potential surface as a harmonic well [9][13].

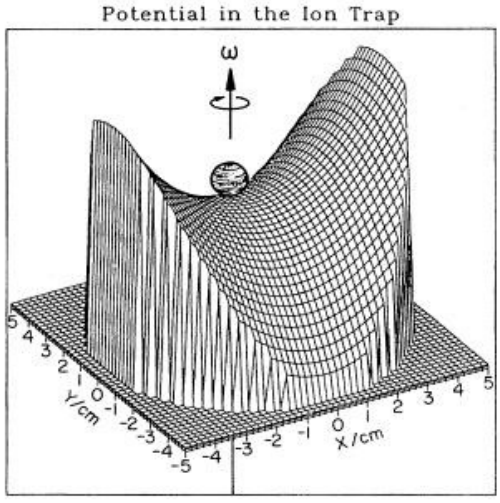

Fig. 1 Illustrates the ion as a ball moving along the approximate surface created within the ion trap [9].

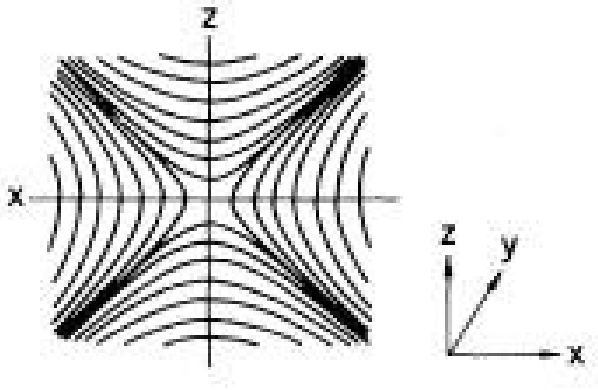

Fig. 2 The potential field lines which are created within a quadrapole trap as viewed axially [9].

A linear Paul trap is used in these experiments to create this potential; the Paul trap consists of four rods, two with static voltages and two with oscillatory RF voltages. It is the oscillatory RF signal which switches the high field regions to low field regions with a cosine waveform. The static voltages on the other two rods are used to compensate for inconsistencies in the field due to defects in the rods as well as uncontrolled fields. This compensation allows for better confinement of the ion which is equivalent to a decrease in the motion of the ion [9].

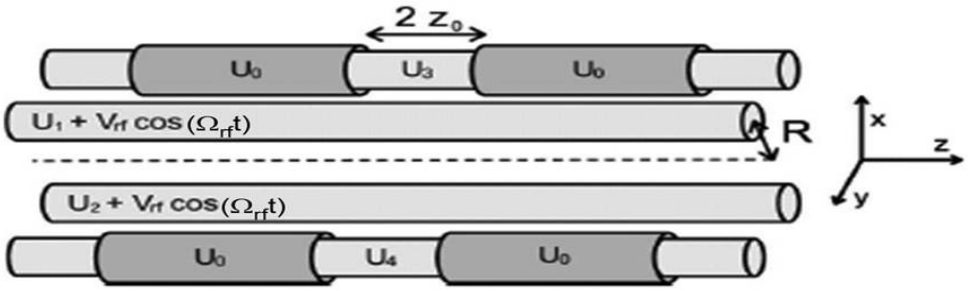

Fig.3 Illustration of a Paul trap the static voltages are zero and the end caps have an applied potential (U_0) which is used for compensation [14].

The stability of the trap can be described by the Mathieu equations, a set of differential equations which describes the motion of the ion within the trap using the dimensionless variables a and q.

$$\ddot{x} + \frac{e}{mr^2}\left[U_0 + V_{rf}\cos(\Omega t)\right] \leftrightarrow \frac{\partial^2 x}{\partial \tau^2} + [a + 2q\cos(\Omega t)] \quad \textit{(Eq. 3)}$$

$$\ddot{z} - \frac{e}{mr^2}[U_0 + V_{rf}\cos(\Omega t)] \leftrightarrow \frac{\partial^2 z}{\partial \tau^2} - [a + 2q\cos(\Omega t)] \quad \textit{(Eq. 4)}$$

$$a = \frac{4eU_0}{mr^2\omega^2}, q = \frac{2eV_{rf}}{mr^2\omega^2}, \tau = \frac{\omega t}{2} \textit{(Eq. 5, 6 ,and 7)}$$

Equations of motion and Mathieu dimensionless representations [9]

These two parameters define the trap stability. The motion of the ion can either be stable or unstable. Stable motion is characterized by amplitudes of motion that are small enough that the ion remains confined to the trapping region and does not come into contract with the electrodes. Unstable motion is characterized by exponentially increasing amplitudes of motion which result in loss of the ion [9].

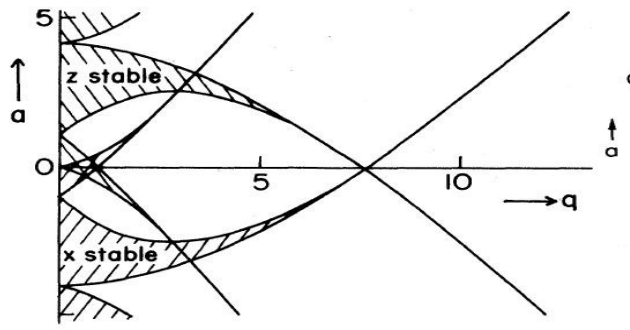

Fig. 4 The two dimensional stability region defined by the parameters a and q [9].

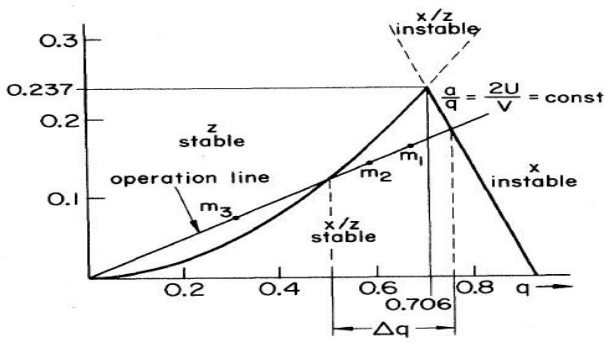

Fig. 5 The x and z stability dependence on mass and the parameters a and q [9].

1.2.2 Calcium Ions

Trapped ions present a promising qubit candidate because of the very long coherence times, on the order of a ms, which can be achieved [15]. A major benefit to using a calcium ion is that it is hydrogenic and can be approximated as one electron orbiting a nucleus. Because of this it is easier to calculate of the energy levels of the system.

The energy level diagram of $^{40}Ca^{+}$ is shown below with the transition to the $D_{5/2}$ state being of particular interest as the optical qubit. The longer coherence time is achieved by taking advantage of the optical qubit transition from the $S_{1/2}$ to $D_{5/2}$ state. This transition is long lived because it is dipole forbidden but quadrapole allowed, and spontaneous emission is dependent upon these selection rules. The lifetime of this transition is 0.77 seconds; meaning that spontaneous emission on average is likely to occur within 0.77 seconds. Spontaneous emission, in reference to the proposed experiments, is a mechanism of decoherence. The lifetime of this state and the gating time of a given operation impose an upper bound on the number of operations that could be performed using that particular state before decoherence occurs.

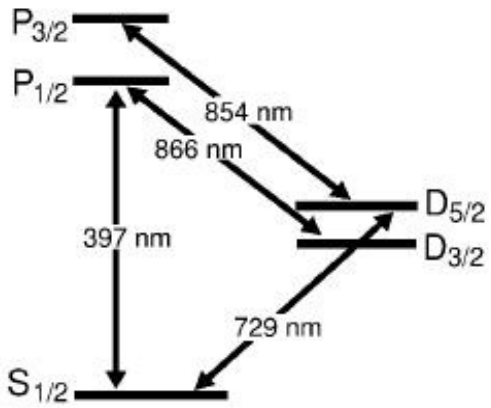

Fig. 6 Energy level diagram $^{40}Ca^{+}$ [16].

This gating time for an optical qubit is based upon the Rabi frequency of the ion radiation interaction, for trapped ions in general this is around 10^{-6} seconds and is dependent on laser intensity. Therefore, it is somewhat arbitrary in this discussion. A quality factor of a given qubit candidate can be determined based upon the ratio of decoherence time and the possible gating time. For the optical qubit transition in Calcium, this quality factor is approximately $7.7 \cdot 10^5$ which is an estimate of the number of operations which could be performed before the qubit state decoheres. Quantum computation theory suggests that for a fault tolerant system, a system which does not collapse due to propagating errors, the inverse of the quality factor must be less than approximately ~10^{-4}-10^{-6} [15]. The inverse of the quality factor of the transition between the meta-stable $D_{5/2}$ and $S_{1/2}$ sate given above is $1.3 \cdot 10^{-6}$. This satisfies the fault tolerant condition.

1.2.3 Laser cooling

Fundamental to the work to be discussed is the laser cooling of trapped ions. Temperature is proportional to the kinetic energy of a body; by reducing the motion of the ion (reducing its kinetic energy) the temperature of the ion is also reduced. The absorption and emission of photons incident or emitted by an ion results in a momentum change. A laser that is incident on the ion and is red detuned from a resonant transition will scatter photons off of the ion when the velocity of the ion is opposite to the wave vector of the incident light. This effect is due to the Doppler shift of the atomic transitions, if the velocity of the ion is small and laser is red detuned then this scattering results in cooling[1]. The direction of emission of a photon is entirely random so when the excited ion drops down to the ground state after emitting a photon this is a directionally random process, over thousands of cycles these events average out to a net zero momentum gain on the part of the ion [11].

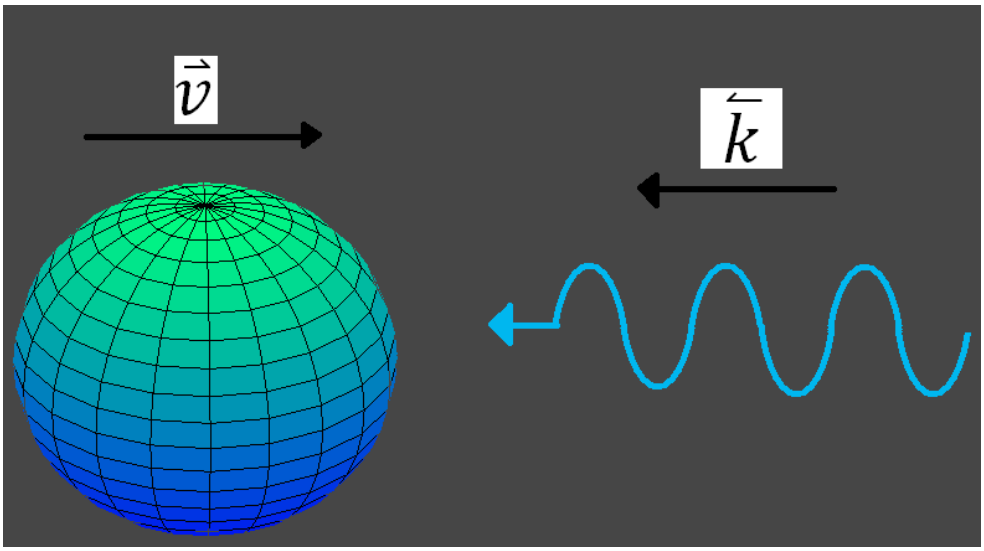

Fig. 7 Schematic of laser cooling showing momentum vectors with the ball representing the atom and the sinusoid representing the incoming laser [11].

The limit to this cooling method (Doppler limit) is fundamentally determined by the natural linewidth of the atomic transitions involved in the cooling process. This limit arises from the maximum scattering force of the radiation on the ion which is determined by the linewidth of the transition. This limiting temperature is approximately in the hundreds of μK. There are several methods of reducing the motion of the ion past this limit. Sideband cooling is the most relevant to these experiments [10].

$$T_D = \frac{\hbar\gamma}{2k_B} \text{ (Eq. 8)}$$

Doppler temperature (T_D), γ is the linewidth of the transition; k_B and $\hbar$ are the normal constants [10].

Chapter II

2.1 Introduction to Lasers

Laser technology is an integral part of most modern physics and chemistry experiments. This is due in large part to the vast number of applications and commercial availability of lasers. In the work discussed here the lasers are all external cavity diode lasers (ECDL)[11]. It will be informative to discuss once again the fundamentals of this device and other techniques needed to implement this type of laser for the experiments being discussed.

2.2 Frequency Control

For spectroscopy of chemical species and coherent control experiments, the stability of the laser frequency and phase is paramount. Two common techniques for stabilizing laser frequency are the side locking method and the Pound Drever Hall (PDH) scheme [19][21]. The idea is to lock the laser to a reference resonant signal from an interferometer; this is accomplished by modifying the laser current and cavity length to maintain a set point at the resonant frequency. The resonant cavity is a Fabry-Perot interferometer.

2.3 Diode

In this type of laser the diode serves as the three level system and the lasing media. The diode is simply a semi-conductor material with both a p and n branch. At the meeting of these two branches equilibrium between holes and electrons is maintained and is known as the depletion region. When a diode is forward biased and current is driven to push electrons towards holes when the electrons fall back down to the n branch a photon is emitted. Therefore the three level system which makes up the semiconductor diode laser is the n branch acting as the ground state, the p branch acting as the higher excited state, and the depletion region or active region acting as the excited state which undergoes stimulated emission. This system is a light emitting diode (LED) below a threshold current, when the population inversion is great enough that photons from falling electrons can cause stimulated emission of other excited state electrons is this a laser. This is the only way in which coherent emission of light can be achieved.

The 729 nm diode used in these experiments was purchased from a commercial diode manufacturer (Eagleyard Photonics). It is a GaAs semiconductor diode which has the circuit structure shown below. The maximum output of this diode is 10 mW at 90 mA. The lowest lasing threshold achieved for this laser diode was 61.9 mA which produces 8 mW of power with an injection current set to 80 mA.

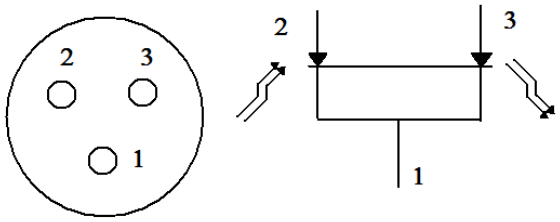

Fig. 18 Left: An image of the diode used in these experiments. Right: (Top) How the pin contacts are numbered. (Bottom) This is a circuit diagram showing the different branches of the diode.

2.3.1 External Cavity Diode Laser (ECDL)

An external cavity diode laser is a semiconductor laser; it consists of two basic solid state elements and a controller. A diode serves as both the source for population inversion, through pumping of current from the controller, and as lasing media. A diffraction grating aligned with the diode serves to create the necessary optical feedback required for lasing to occur. The controller sets the injection current sent to the p-n junction of the diode as well as temperature stabilizes the entire apparatus. In the following section these three elements will be discussed in terms of how each one contributes to the lasing threshold, the stability of the laser, and any specific elements in the ECDL.

2.3.2 Diffraction Grating

The diffraction grating serves as one of the surfaces forming the laser cavity for an ECDL. As mentioned in the diode section, this set-up is a laser when previously emitted photons can cause stimulated emission of excited state electrons in the gain medium; this is the only way coherent light amplification can occur. If the diffraction grating is aligned in such a way that there is optical feedback towards the diode creating a cavity these photons can cause stimulated emission and lasing will occur.

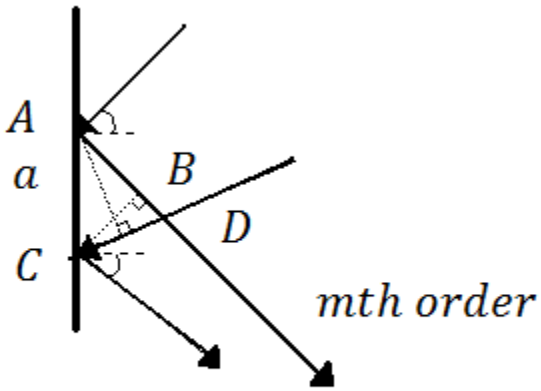

$$AB - DC = a(\sin(\theta_m) - \sin(\theta_i))$$

Fig. 9 Dependence on the angle of incidence on beam order [11].

$$a(sin\theta_m - sin\theta_i) = m\lambda \ (Eq.\ 9)$$

The relation between beam order (m), angle of incidence (θ_i), angle of deflection (θ_m), and wavelength (λ) [11}

Diffraction gratings consist of a highly reflective crystal with periodic minute grooves, when light is incident upon a diffraction grating interference occurs and beams of several orders (m) are deflected off of it. The angle of deflection of a given beam which is not of order zero ($m \neq 0$) is wavelength dependent, by adjusting the position of the diffraction grating the laser is tunable over the range of wavelengths that the diode can emit. The diffraction grating in this laser is characterized by having 1800 grooves/mm and a grating constant, *a*, of 556. This makes the angle of deflection with reference to the grating normal ~81^0 using the equation above, this is the angle which will deflect the m=-1 beam back towards the diode.

2.3.3 Control System

The control system is commercially available and is not modified in the implementation of this experiment; however it is worth mentioning because it contains all of the electronics which operate the laser. The controls for modifying and setting limits on the injection current are a part of this system as well as the controls which maintain the diode temperature. The diffraction grating is attached to a piezo which can change the length of the laser cavity which changes the frequency of the laser, the voltage and sweeping controls for this piezo are found in the control system. This system also houses the electronics used for locking the laser (FALC 110) which will be discussed later. It appears here only to define it as part of the operating elements of the ECDL laser.

2.4 Interferometers

The frequency stabilization of the ECDL was experimentally very involved and required the design of new laboratory elements, most importantly an interferometer with an extremely narrow transmission frequency. This is the frequency which is used as the reference for locking the ECDL frequency. The main body of experimental work thus far has been in the implementation of this high resolution optical cavity. This section will cover the relevant fundamentals of interferometry work as well as specific aspects of the design for this experiment and the success of that design.

2.4.1 Introduction to Optical Resonators

An interferometer by definition is a device which can be used to measure the interference between two waves. The interferometer used here was a Fabry-Perot interferometer which in the simplest form consists of two plane parallel highly reflecting surfaces. Any light which is inside the region between these two surfaces and traveling along the optical axis of these surfaces would theoretically be indefinitely trapped within this cavity. A traveling wave propagating through this space will have a phase shift imparted to it after reflecting off one of the two surfaces, therefore only light waves that can fit an integer number of wavelengths within the region between the two surfaces will not deconstructively interfere. Light waves that meet this condition will form standing waves within the cavity.

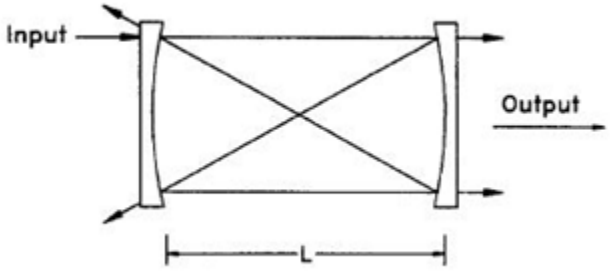

Fig. 10 A Fabry-Perot interferometer, this interferometer is a spherical confocal cavity [17].

If one of these surfaces will partially allow light to enter the cavity and one of these surfaces will allow a very small amount of light to exit; then an incident laser beam with an oscillating frequency which will transmit only one frequency through the cavity. This frequency is dependent on the wavelength of light and the length of the cavity. Therefore the interferometer can be used as a frequency reference. This is how the Fabry Perot cavity in this work is used to stabilize the laser. The level of stabilization which can be achieved is dependent on the specificity of the cavity resonance. This is determined by a quantity known as finesse (F); the finesse of the cavity is the number of round trips a photon of a given frequency must make before being transmitted through the cavity. The finesse is a function of the reflectivity of the faces of the two surfaces which form the cavity. The higher the reflectivity the higher the number of passes which must be made before transmission. The frequency spacing between transmission peaks is known as the free spectral range (FSR) and is determined by the length of the cavity. The width of the transmitted cavity mode in frequency space (specifically its full width at half max) is related to the finesse by the FSR.

$$F = \frac{\pi\sqrt{R}}{(1-R)} \quad \textit{(Eq. 10)}$$

$$\Delta\upsilon_{FSR} = \frac{c}{4nL} \textit{(Eq. 11)}$$

$$\Delta\upsilon_{FWHM} = \frac{\Delta\upsilon_{FSR}}{F} \textit{(Eq. 12)}$$

Top to Bottom: Finesse, F, where R is the reflectivity, Free spectral range, FSR. c is the speed of light and L is the length of the cavity,, and the full width at half maximum of the transmitted signal, Δυ [13]

2.4.2 Cavity Assembly and Vacuum Chamber

Using plane faced mirrors is extremely difficult, any deviation from the optical axis will create a catastrophic loss of signal (the signal will not be transmitted but escape outside of the cavity), and similarly any deviation between the optical axes of the two surfaces will cause the same efficiency issue. This problem is only compounded when using a high finesse cavity, the more trips the more impact a small deviation makes. This difficulty can be overcome by using spherical confocal mirrors (Fig.13) to focus the reflected beams towards the center of the cavity. This means the confocal cavity is much easier to align. Perfectly confocal resonators have a degeneracy which changes the denominator of the free spectral range relation from 4nL to 2nL [20]. This degeneracy arises because all of the transverse cavity modes will be symmetric about the cavity center.

In the apparatus used in these experiments the cavity is a confocal resonator but the focal point of either mirror is longer than half way between the two. Therefore the degeneracy of the confocal cavity is lost. The mirrors which are used are highly reflective (99.997% reflectivity) to achieve an extremely high finesse. These mirrors are connected to each other by an ultra low expansion material and two piezo electric rings which allow for minute controlled changes in the length of the cavity. Two rings are used so that if there is some deviation of the applied signal or some natural offset of the piezo it will be canceled by the same deviation in the other piezo.

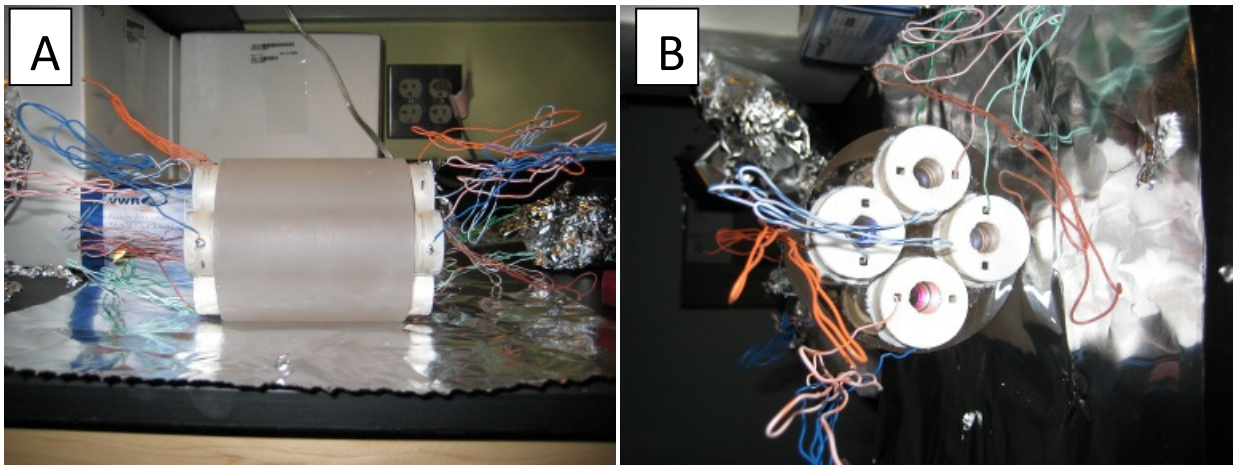

Fig. 11 A: Side views of ULE cavity, the rings are individual interferometers. B: Front view of the cavity, the back faces of the mirrors can be seen in each of the four holes surrounded by the white rings

The ultra low expansion material (ULE) has a maximum coefficient of thermal expansion of $60 \cdot 10^{-9}$ K. The temperature fluctuations of the room range from 24-26 ^{0}C. Minimizing temperature fluctuations is extremely important when trying to achieve high finesse, the deviations in length of the cavity scale linearly with the fluctuations in frequency width of the transmitted signal.

The cavity was hung within a vacuum chamber to ideally block out vibrations, additional thermal fluctuations, but most importantly to achieve constant index of refraction between the two cavity mirrors to a high degree of precision. Changes in index of refraction can also cause major deviations in frequency width for the same reasons that temperature drifts also cause major fluctuations.

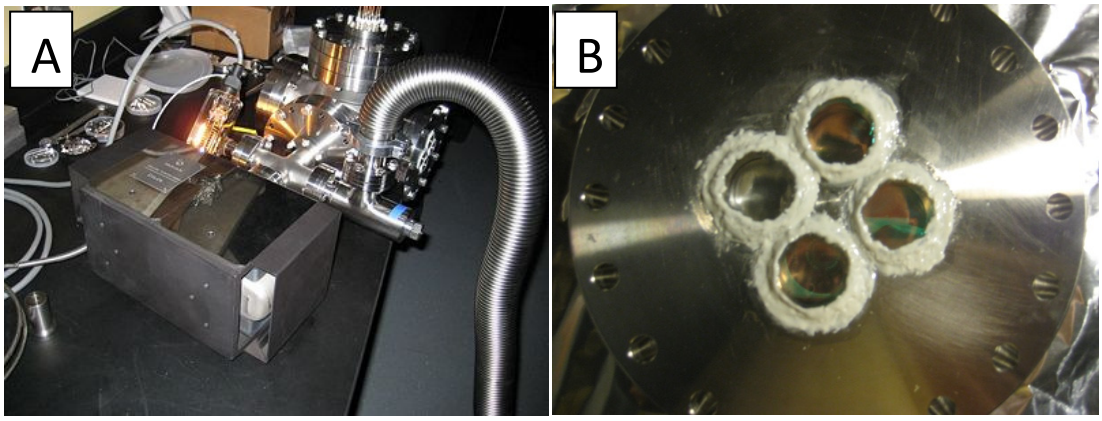

Fig. 12 A: View of the vacuum apparatus and pump B: Front view each window corresponding to each individual cavity

2.4.3 Results

By using a CCD camera and examining the transmitted mode through the cavity a TEM_{00} mode was optimized. Once it was clear that the TEM_{00} was being selected, several tests were done to determine the success of the cavity assembly. By tuning the piezo, which controls the diffraction grating of the laser, a range of frequencies were scanned to determine the FSR of the cavity. By using a fast oscilloscope and a calibration curve the FWHM was also determined. The finesse of the cavity was roughly estimated by these values. A more accurate measurement of the finesse was achieved by performing a cavity ring down experiment. In this experiment the laser is quickly shifted from the cavity resonance and then back again to generate a series of decaying exponentials. The decaying exponentials represent the signal diminishing as light quickly leaks out of the cavity. These decaying exponentials where then used to determine the lifetime of light within the cavity, considering the cavity to be in vacuum and knowing the exact length of the cavity from the FSR, the number of round trips the light must make inside the cavity was calculated. This value corresponds directly to the finesse of the cavity. The exponential used to calculate the finesse is given below and calculated an average finesse of approximately 90,000.

$$f(t) = Ae^{-t/\tau} + C \quad \textit{(Eq. 13)}$$

Decaying exponential used to calculate finesse. A is the amplitude, C is an offset which is set to zero and τ is the time constant which is of interest

2.5 Laser Locking to Resonators

High finesse optical resonators can be used to stabilize the ECDL. The frequency band of the laser can be narrowed and a specific frequency can be locked. This can be done by locking the laser to the cavity resonant frequency and using a feedback loop to keep the laser at that frequency by modulating the injection current. Previous work focused on side locking mechanisms, these were shown to be insufficient at stabilizing the laser. A Pound Drever Hall lock circuit would allow for increased laser stabilization as well as phase control, which is necessary for dynamic decoupling pulse sequences.

2.5.1 Fundamentals

Two common lock designs are the Pound Drever Hall (PDH) and the side locking method. Both of these methods make use of an optical resonator as the source of the reference frequency for the locked frequency of the laser. In the set-up used in these experiments both of these methods made use of a fast analog linewidth control circuit (FALC) which acts as a high-speed control amplifier. It consists of several frequency filters that amplify different frequency regions of an error signal which is generated from a given input signal. The filters are set up as integrators and differentiators acting in tandem much like a PID lock.

A side locking system for a diode laser makes uses an inferometer and photodiode coupled to several fast acting electronic filters (FALC) that are then coupled to the current of the laser diode. The electronics read a change in a set frequency of the cavity and modulate the current of the laser to maintain a set point. The disadvantages of this method are that fluctuations of the laser diode may cause instability in the lock, and the inability to lock to the maximum intensity of the resonance frequency. The set point must be locked to either side of resonance or have room to move towards or away from resonance without moving over it in order to maintain the lock; this limits how far the linewidth of the laser can be narrowed.

In the Pound Drever Hall system, the laser phase or frequency is modulated before a Fabry Perot cavity. The reflected beam off of the front face of the Fabry Perot cavity is detected by a photodiode, this signal is then sent through a low pass filter to select the region of frequency interest, the signal is then mixed with the phase or frequency modulation trigger applied to the laser before the Fabry Perot cavity. The output signal of the mixer will be anti-symmetric about the cavity resonance. The error signal that results is sent to a phase or frequency detector which then tries to maintain the zero in the highest slope region by adjusting the laser through current modulation [19]. This allows for high frequency stabilization as well as phase control. This technique is commonly used for high frequency stabilization in the search for gravitational waves [20][21].

2.5.2 Side locking

In initial experiments side locking was used to stabilize the laser frequency. This method highlights many stability issues with the cavity set-up which were mitigated by monitoring the effects of optimization on the side locking type frequency lock.

It was discovered that temperature fluctuations in the room were causing major fluctuations in the stability of the laser lock. For this reason a temperature controller was purchased, which used heat conductive tape wrapped around the vacuum housing. This temperature controller is given a set point temperature to maintain and reads the temperature at an arbitrary point on the cavity housing. It then tries to maintain this set point, in a PID type fashion, by increasing or decreasing the current applied to the conductive tape. By optimizing the PID settings of this temperature controller major gains in the laser stabilization were achieved.

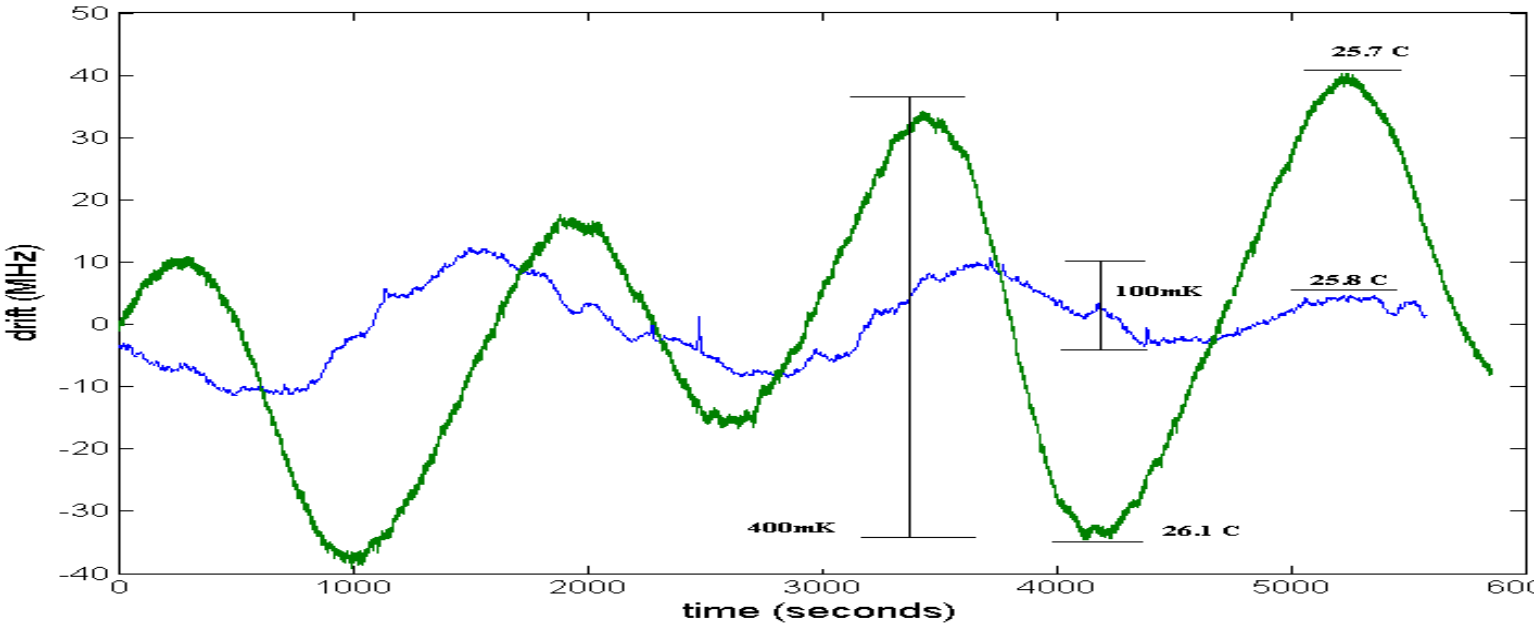

Fig. 13Drift in frequency of the locked laser at different temperatures without any kind of temperature stabilization the blue curve is at 28.8 ^{0}C and the top curve is 28.7 ^{0}C.

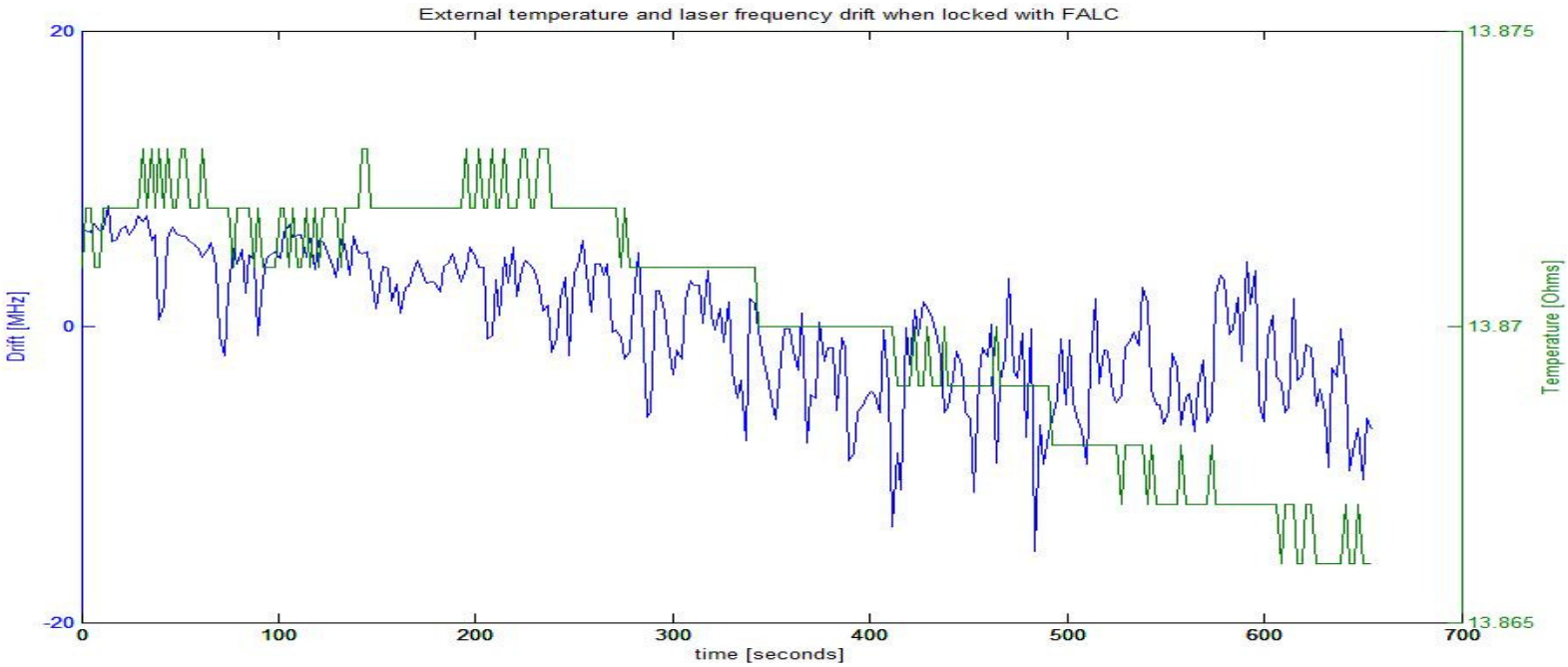

Fig. 14 The green curve shows a change over time in temperature and the blue curve represents the drift in the locked laser frequency over this same time period, showing that after optimization the locked frequency is much more decoupled from temperature than it was before.

Interest in testing the dynamic pulse sequences which is the subject of this thesis meant that the side locking method was insufficient and therefore abandoned. This was mainly done because the side locking method did not adequately narrow the linewidth of the laser.

2.5.3 Pound Drever Hall Details

The PDH lock required the design of a lock circuit and a new optical layout. The chosen Pound Drever Hall lock uses an electro optical modulator (EOM) coupled to a resonant circuit and local oscillator as the sideband source. An EOM is a crystal that when an electric field is applied to the crystal the polarization of laser light passing through the crystal will change[19]. By coupling the EOM to a resonance circuit and driving it at some known frequency sidebands are generated on the cavity transmission signal. In this set up these sidebands should be 20 MHz away from the carrier peak [18][21]. A diagram of the exact implementation used in this discussion is shown below. This diagram also serves as a reference for all other optical elements within the set up.

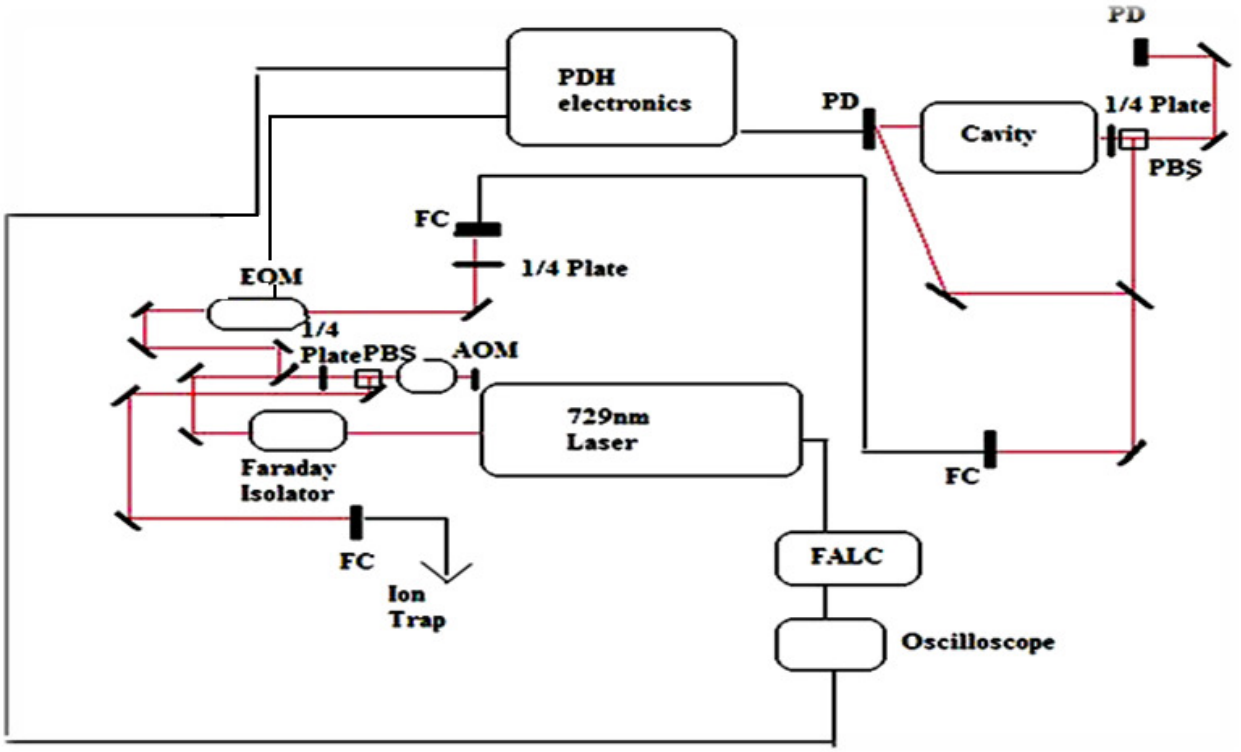

Fig. 15 Optical layout of the 729 nm laser system.

The application of the 20 MHz sidebands to the carrier transmission cavity peak has been shown. From this an error signal has been generated and the phase has been optimized, these two waveforms are shown below. Optimization of the FALC has led to a stable PDH lock which narrows the linewidth of the laser below the error threshold of the wave meter used in current experiments. A better determination of the laser linewidth will come from measurements of a trapped Calcium atom which serves as the absolute reference for all the experiments done and proposed in this thesis.

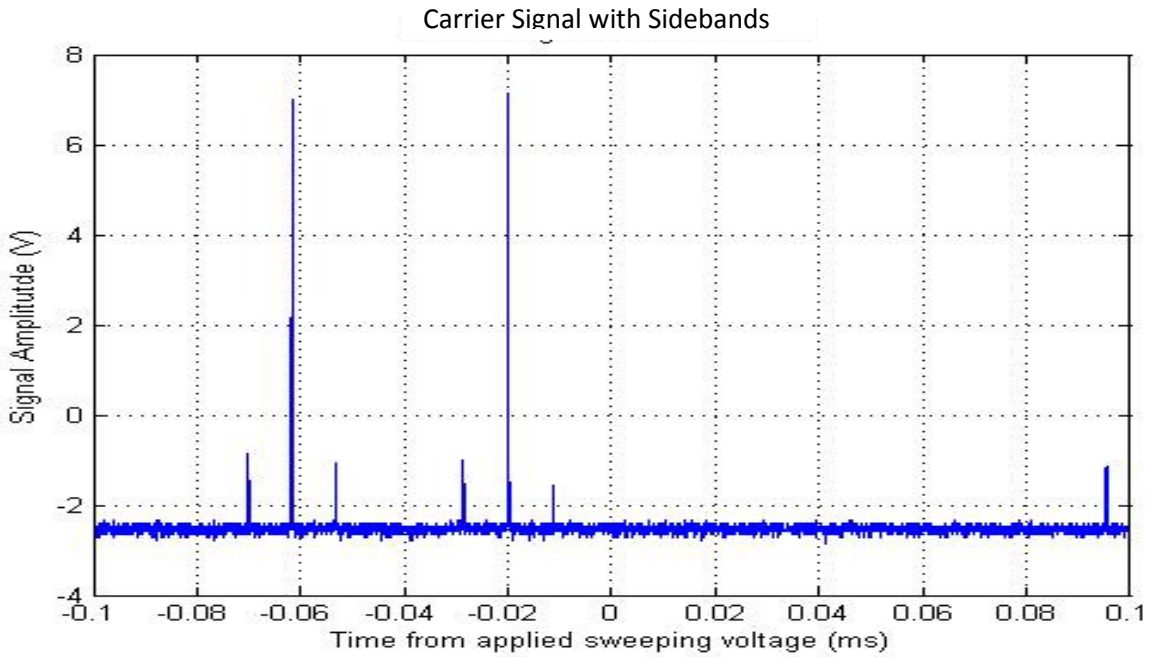

Fig. 16 Plotted waveform of the balanced transmitted signal, this is the difference signal between the transmission signal and a beam which is not incident on the resonator. The large amplitude peak is the carrier signal. The two sidebands are observed approximately 20 MHz away, the smaller amplitude peaks.

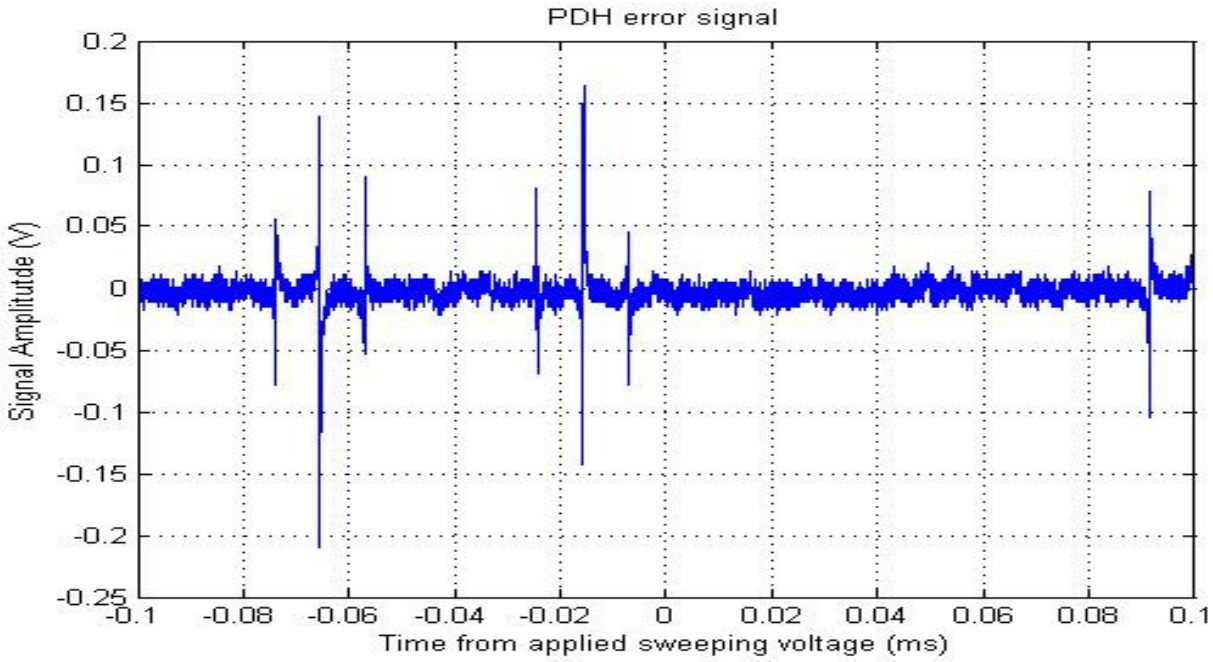

Fig. 17 Plotted waveform of the error signal produced from the signal shown in Fig. 19.

To understand the difference between the side locking and PDH scheme consider the different widths of the lorentzian carrier shown in Fig 19. Side locking effectively locks the laser to either side of this resonance as opposed to the PDH in which the laser is locked to the maximum value of this resonance.

The plot below shows the drift in frequency of the laser locked by the PDH scheme versus the number of sideband data sets taken; this plot indicates the long term deviations from a given set point. Current estimates put the linewidth of the laser to be less than tens of kHz, this should be sufficient to resolve the motional sidebands which should have spacing of approximately a MHz. Each slice is a measurement of the motional sidebands of the trapped ion. The motional sidebands correspond to states dressed by the motion of the ion in the potential. Locking the laser frequency to the sidebands is the next step in a procedure to perform a spin-echo experiment.

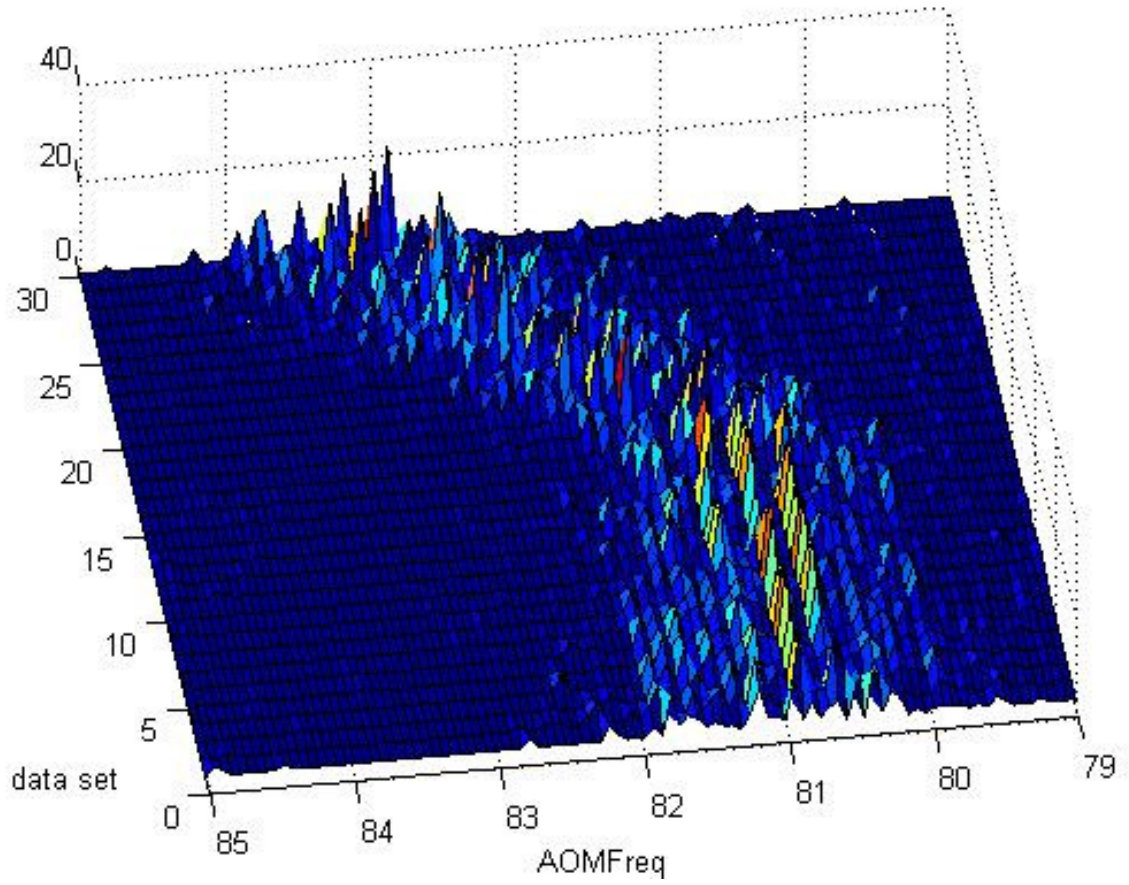

Fig. 18 Plotted three dimensional drift of the laser with respect to the positions of the sidebands. The slow drift is due to temperature fluctuations in the laboratory. The AOM frequency is double that of the actually frequency.

Chapter III

3.1 Dynamic Decoupling

Dynamic decoupling pulse sequences provide an interesting new approach to arbitrary qubit error correction. The spin of a given qubit can be considered as a state vector pointing from the origin to the given state of the system. By only considering the spin state of the system, the qubit state is confined to motion on a sphere, rotations. If an appropriate pulse or pulse sequence can then be applied to a qubit which is undergoing some decoherence rotation such that the time reversal process occurs the system will return to its original state. The power of this technique arises from the constraint of rotations on a sphere. In this space the path of the state does not need to be known only how to get back. Errors in the state preparation of the system can be corrected by determining pulses which create a set of rotations to return the system to the initialized state.

These types of techniques have been understood since the 1950's but were mainly developed in the field of nuclear magnetic resonance (NMR) spectroscopy [4][8]. In that situation Larmor free precession causes the spin state of the molecules of interest to longitudinally relax destroying the resolution of a given spectrum. In 1950 it was discovered that an appropriate RF pulse causes a rotation of the state and at some time later an echo of the original spin state is observed. This is known as spin echo, and was the basis for the original pulse sequences which were developed, this section will discuss several of those sequences and how to implement them in the experiments proposed in this thesis.

3.1.1 Hahn (Spin) Echo

The spin echo phenomenon is the fundamental basis for all dynamic decoupling pulse sequences. This concept can be better understood if the system at hand is considered to be an ensemble of spin states; by applying an appropriate magnetic field or RF pulse the ensemble will assemble into a given spin state. Due to in-homogeneity of the magnetic field these spin states may begin to move to another spin state (decoherence), and this may happen to certain spins more readily than it does with other spins. However there exists some operation which will take the spins along a similar path to that of the decoherence path and recombine them in a given spin state. One way to visualize this effect is to consider the spin state vectors as being centered at the origin of a sphere (Bloch sphere) where the poles of the sphere are the pure spin states and the states on the equatorial line are the superposition states with equal mixing, transitions between spin states can be visualized as rotations on this sphere [4][8].

This is the best picture to view the most basic of dynamic decoupling experiments which consists of an applied pulse and an echo measurement. The figure below depicts the Bloch sphere of the Hahn echo pulse, in this experiment the spin states are initialized in the + y direction by applying a pulse that will cause a $(\pi/2)_x$ rotation about y, after a given time τ due to unavoidable coupling to the environment the spin states will decohere into a mixture of + x and – x states. At this point by applying another $(\pi/2)_x$ pulse the states will condense to the –y state after the same time τ. The original application of this pulse was in the field of NMR resonance where the rotations were achieved by applying the appropriate idealized RF pulse. In the experiments proposed here the states (y, x, and z) would correspond to states reached through an optically pumped transition, rotations will be achieved by pulsing laser light.

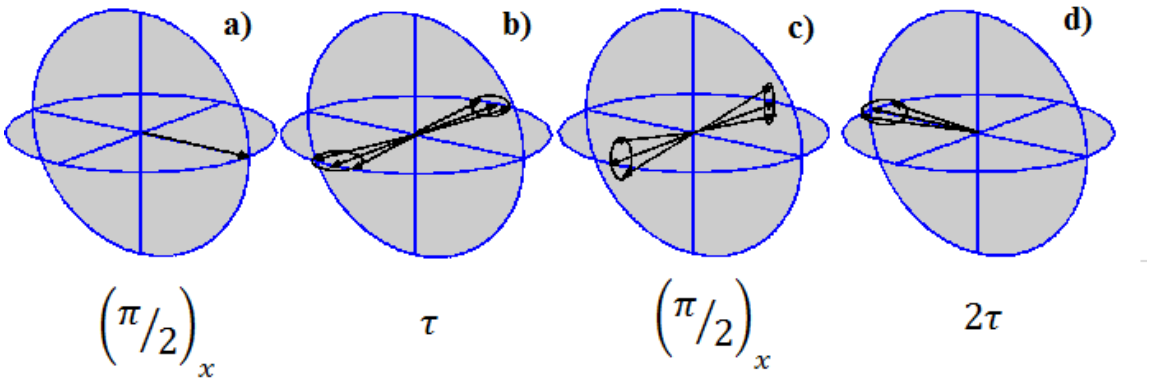

Fig. 19 Bloch sphere representations of the spin state vectors at different points in the Hahn echo experiment. (a) is the initialization of the vectors in the y axis, (b) shows the dephasing in the xy plane which occurs over a time τ, (c) shows the effects of the $(\pi/2)_x$ rotation pulse (d) depicts how dephasing returns the vectors to the –y axis after time 2τ from the applied pulse [8].

3.1.2 Carr-Purcell-(Meiboom-Gill)

The Carr-Purcell pulse experiment is the first to truly mitigate decoherence. In the Hahn Echo experiments, half of the spin states are not refocused to the –y state, losing half of the information is unacceptable. The Carr-Purcell pulse uses a $(\pi)_x$ pulse to refocus the spin vectors into the –y state. The major advantage of this pulse is that it focuses all of the spins to the –y state and it can be applied at any time as opposed to the Hahn echo where it is essential that the spin states are spread out over the xy-plane before the refocusing pulse is applied (this is why time τ must pass before applying the pulse). Because of this an attempt was made to maintain constant coherence by successively applying these pulses, however because these pulses contain error the rotations are not exact. Successive application of these rotations causes an accumulation of these errors resulting in eventual loss of state coherence [8].

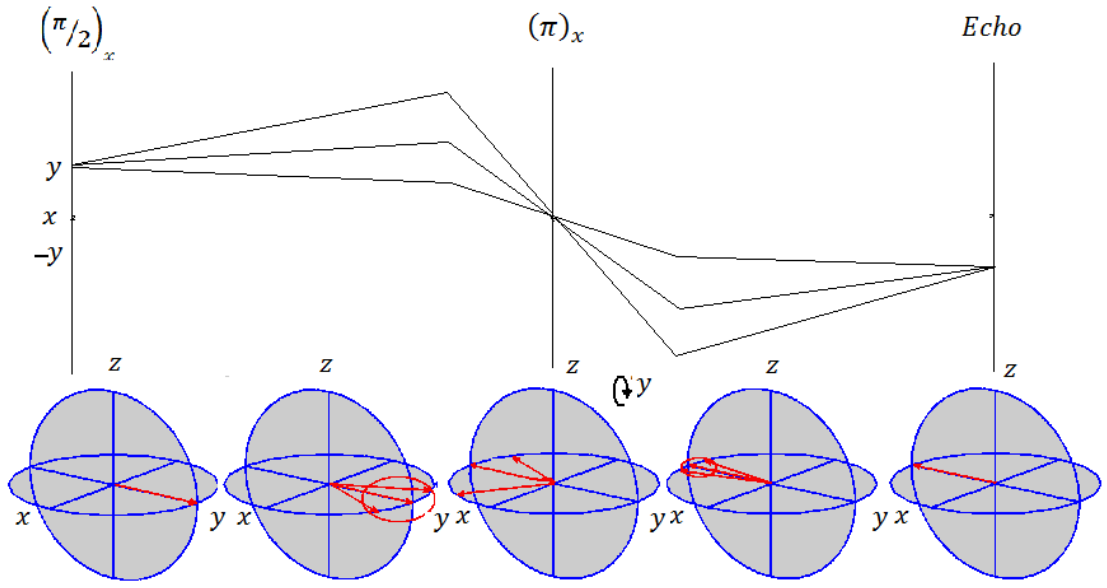

Fig. 20 The Bloch sphere and the longitudinal position of the state vectors in the Carr- Purcell pulse sequence. The far left line represents state initialization in the y axis, the block sphere in between this line and the next depicts the dephasing. The center line represents the application of the $(\pi)_x$ pulse, and the last line shows refocusing to the –y axis [8].

The Meiboom-Gill modification takes advantage of the same principles that make the spin echo phenomenon possible by applying a $(\pi)_y$ pulse as opposed to a $(\pi)_x$. This pulse will also introduce errors to the desired rotation, however it will do so in both positive and negative deviations from the desired axis of rotation. This type of spin echo experiment is at the heart of all dynamic decoupling sequences which are being studied today.

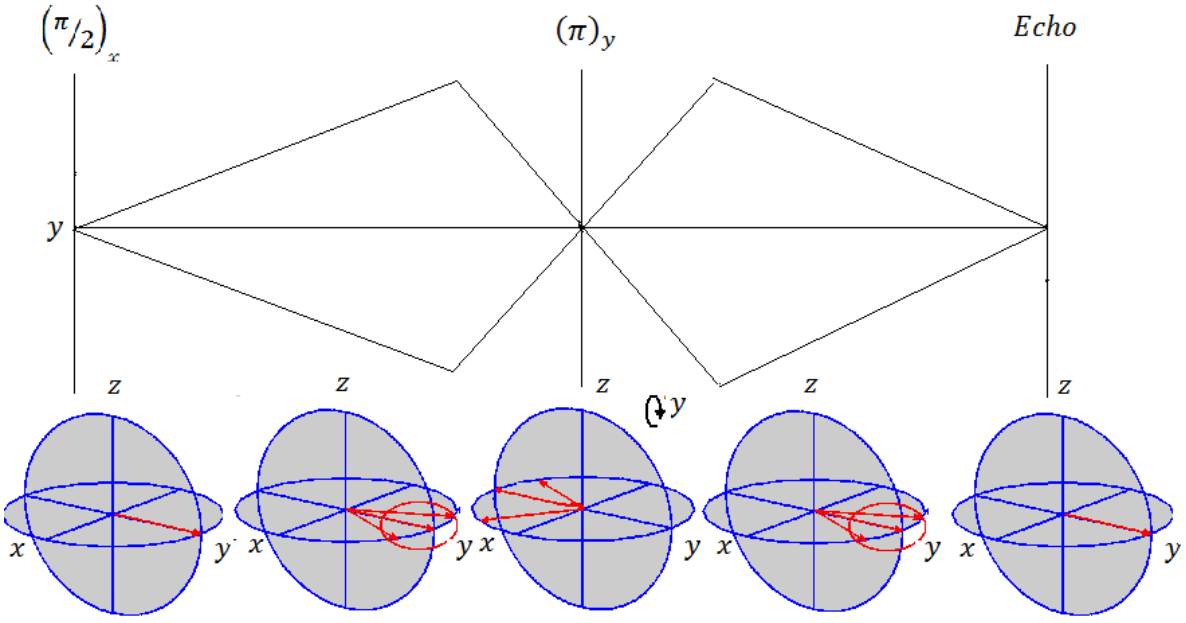

Fig. 21 The dephasing and refocusing of the Carr-Purcell pulse sequence with the Meiboom-Gill modification [8].

3.1.3 Modern Pulse Sequences (CDD and UDD)

The methods discussed above can be applied to mitigate decoherence due to dephasing using rotations about x. Neither of these methods is very robust against initial state errors or spin bath coupling which introduce arbitrary rotations. Rotations about the z axis will cancel out longitudinal relaxation decoherence. By sequentially applying a set of these x type and z type rotations arbitrary errors can be mitigated to a given order. This universal sequence of pulses can be written as fXfZfXfZ where f represents the time between pulses, X and Z represent π rotations about the given axis [3]. Successively applying this pulse sequence will mitigate the highest order term in an expansion of arbitrary error (Magnus expansion) [5]. This pulse scheme achieves first order decoupling by only using 4n pulses, however the higher order error terms are non-trivial and must be addressed.

Concatenated dynamic decoupling works by recursively embedding the pulse sequence given above into each pulse free time f. Each level of concatenation mitigates a higher order term in the error expansion. In this way CDD can mitigate errors to an arbitrarily high order, however the number of pulses required to decouple an n order error grows exponentially as 4^n. Although the nature of the embedded pulse sequence does much to loosen the requirement of idealized pulses, the number of pulses required for this scheme is quite large [3][5][6][7].

$$O_0=f$$

$$O_1=O_0X\ O_0Z\ O_0X\ O_0Z$$

$$O_n= O_{n-1}X\ O_{n-1}Z\ O_{n-1}X\ O_{n-1}Z$$

CDD concatenation scheme [2]

In contrast to the CDD pulse sequences which obtain arbitrary order decoupling through a massive amount of pulses another pulse sequences exists developed by Götz Uhrig which optimizes the time f between the pulses in a CPMG type pulse sequence, this achieves a universal decoupling for the pure dephasing model [22][23]. It has been shown that due to symmetries in the decoupling operations the UDD pulses can also correct for longitudinal relaxation by applying respective Z type rotations as opposed to X rotations [24]. By concatenating these two sequences (CUDD) universal dynamic decoupling of both dephasing and longitudinal relaxation can be achieved to n order of the error expansion by applying $n \cdot 2^n$ pulses [25]. Not only does this makes CUDD a more viable solution, but UDD is also the only pulse sequence which has been shown to mitigate decoherence of a trapped ion qubit experimentally (solid state dynamic decoupling has also recently been shown)[26].

Chapter IV

4 .1 Conclusions

Current experiments are limited by the thermal fluctuations in the laboratory, however the sidebands of the ion can be resolved. The plot below is a scan indicating the motional sidebands corresponding to the particular secular frequencies of the trap. The width of these transitions is broadened due to fluctuations in the magnetic field

as well as other environmental coupling. An estimate of the size of this fluctuation can be made by determining the width of these peaks. This width gives an idea of the scale of fluctuation which we would like to overcome by applying a dynamic decoupling sequence. In the plot shown below the peaks are approximately 100 kHz wide. Fluctuations of this scale are equivalent to fluctuations of about 60 mG in the magnetic field. This can be calculated by estimating the fluctuations in the Zeeman energy shifts [1]. By applying decoupling pulses we would want to get rid of this field.

$$\frac{\mu_B \Delta\omega}{g_J h} = \Delta B \quad \textit{(Eq. 14)}$$

By writing the Bohr magneton in terms of a frequency this is straightforward calculation we take into account the Lande g_J factor because this is a $D_{5/2}$ state and we are in the anomalous Zeeman region [1].

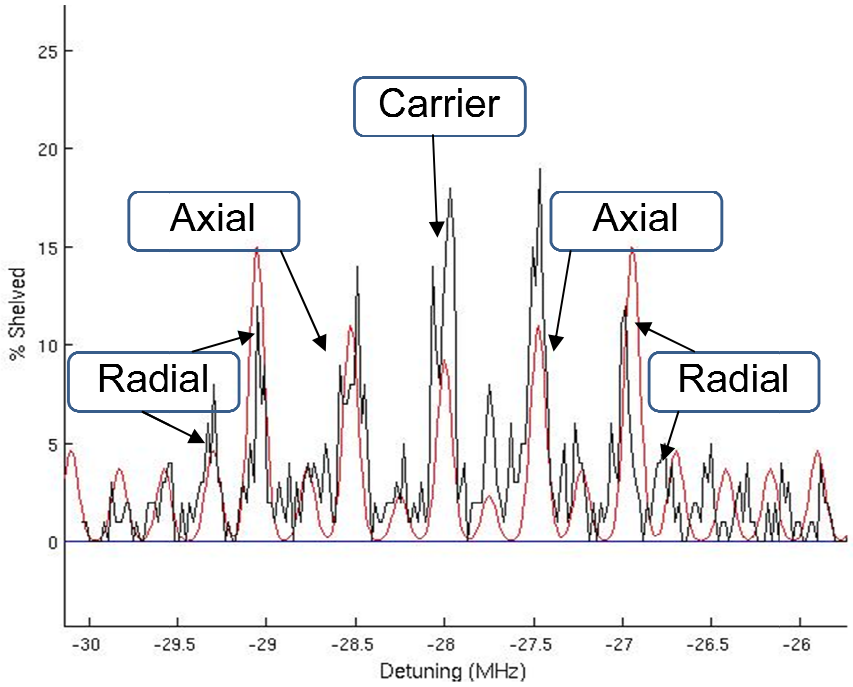

Fig. 22 This is a scan of the motional sidebands of the trapped ion. The AOM shown in the optical layout is scanned over range of frequencies and the shelving percentage to the $D_{5/2}$ state is measured. The labels indicate the motion which is being addressed.

The goal of this research is to be able to mitigate these fluctuations to an arbitrary order and therefore prolong the coherence time of the ion significantly. By improving the coherence time to a range much greater than a μs the calcium ion would surpase the longest coherence times achieved in solid state systems, another possible qubit system. This advance would represent a significant step towards solving a current problem in scalable quantum computing using trapped ions.

4 .2 Future Work

Nearly all the dynamic decoupling schemes discussed until now have not been shown experimentally (this is excluding UDD) therefore the major expansion of this work will come from experimental implementations of

these pulse sequences. As of yet only the UDD type pulses have been tested experimentally and only for Be^+ trapped ions using a hyperfine qubit and for solid state samples which have not been considered here (solid state qubits suffer from an entirely new host of decoherence mechanisms)[26]. CDD has not yet been compared to CUDD or any other pulse sequence experimentally, and such an experiment would largely validate numerical calculations of the superiority of the UDD pulse sequence. There are also novel pulse sequences still being developed which vastly decrease the pulse costs to obtain arbitrary error correction, experimental implementation of pulse sequences of this type may actually provide proof of concept that this type of decoherence mitigation can be used in a quantum simulator.

4.2.1 Experimental CDD

An experimental comparison of CDD and UDD could validate the numerical approximations which have been coming out for the last decade. If compared to the direct UDD type experiment this comparison might give interesting insight into what is a more difficult experimental problem to overcome, longitudinal relaxation or higher order arbitrary error terms. If it appears that only a few orders of error need to be corrected for and that longitudinal relaxation is a difficult experimental problem, CDD could be shown to be a viable decoupling scheme. Another interesting experiment would be to try and use CDD as a way to maintain the coherence of an optical qubit as opposed to a hyperfine qubit; this is most likely where the research presented in this thesis is heading.

4.2.2 Experimental UDD

The Uhrig dynamic decoupling has thus far been the only decoupling sequence which has been shown to mitigate decoherence errors of a trapped ion hyperfine qubit. These results showed that the UDD pulse sequence was much more robust to initial state errors than was a CPMG type pulse sequence. This is what would be expected, however the two pulse sequences performed very similarly in mitigating errors in the xy plane of the Bloch sphere. It would seem entirely possible to attempt these experiments using CUDD and make a comparison, as of yet this has not been done. Also considering this is the only sequence which is known experimentally to maintain coherence; attempts to maintain the coherence of other qubit systems, specifically optical systems could be an interesting expansion [26].

4.2.3 Experimental QDD

Recently a new dynamic decoupling scheme has been introduced which would appear to be very achievable in the laboratory, It is known as quadratic dynamic decoupling. The main feature of the pulse sequence is that it optimizes the time between pulse intervals of a CUDD type pulse sequence which mitigates dephasing and relaxation. This pulse sequence has been numerically shown to far outperform any pulse sequence proposed thus far; a particularly enticing advantage is that mitigation of n order error is achieved by applying only n^2 pulses. Making this pulse sequence by far the most achievable at maintain state coherence for an indefinite period of time, experimental studies of this technique would not be much more difficult than performing the UDD type experiments. An excellent experimental result would be to test this pulse sequence on a trapped ion to compare with the results of the UDD experiments, the only difficulty would be the level of accuracy in the clocks used in determining the time intervals between pulses [25].

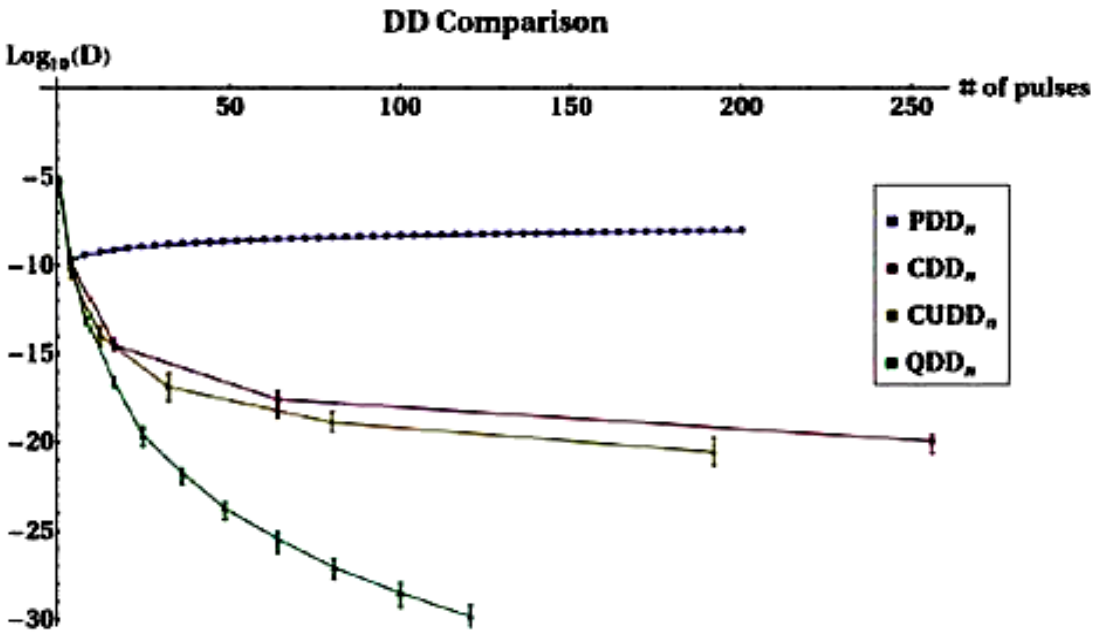

Fig. 23 This is the numerical results of the QDD type pulse sequence as compared to other dynamic decoupling schemes, D on the y axis is the range on the fidelity and can be thought of as a measure of the fidelity [25]

References

[1] “Atomic Physics” C. Foot, Oxford Press, New York 2005

[2] "Fault-Tolerant Quantum Dynamical Decoupling" K. Khodjasteh, and D. A. Lidar, Phys. Rev. Lett., 2005, 95

[3] "Performance of Deterministic Dynamical Decoupling Schemes: Concatenated and Periodic Pulse Sequences" K. Khodjasteh, and D. A. Lidar, Phys. Rev. A, 2007, 75

[4] "Spin Echoes" E. L. Hahn, Phys. Rev., 1950, 80

[5] "Concatenated dynamical decoupling in a solid-state spin bath" W. M. Witzel, S. D. Sarma, Phys. Rev. B, 2007, 76

[6] "Concatenating Dynamical decoupling with decoherence-free subspaces for quantum computation" Y. Zhang, Z. W. Zhou, B. Yo, and G. C. Guo, Phys. Rev. A, 2004, 69

[7] "Concatenated Control Sequences based on Optimized Dynamic Decoupling" G. S. Uhrig, Phys. Rev. Lett., 2009, 102

[8] “Spin Choreography: Basic Steps in High Resolution NMR” R. Freeman, Oxford Press, New York 1997 pp. 108-117

[9] “Electromagnetic traps for charged and neutral particles” Wolfgang Paul, 1990

[10] "Laser Cooling and Trapping" Harold J. Metcalf; Peter van der Straten. Springer Verlag, New York . 1999 pp. 63-65

[11] "Optics" E. Hecht, Pearson Education, 2002

[12] "Introduction to Electrodynamics" D. J. Griffiths, Pretince Hall, Upper Saddle River, New Jersey 1999 pp. 111-114

[13] "Depletion, Quantum Jumps, and Temperature Measurements of $^{88}Sr^{+}$ Ions in a Linear Paul Trap" P. Richerme, MIT thesis, 2006

[14] "Minimization of ion micromotion in a Paul trap" D. J. Berkeland, J. D. Miller, J. C. Bergquist, W. M. Itano and D. J. Wineland, Journal of Applied Physics, 1998, 83

[15] "Multi-pulse coherence enhancement of solid state spin qubits" W.M. Witzel and S. Das Sarma, 2008

[16] "Quantum State Engineering on an Optical Transition and Decoherence in a Paul Trap" Ch. Roos, Th. Zeiger, H. Rohde, H. C. Nägerl, J. Eschner, D. Leibfried, F. Schmidt-Kaler, and R. Blatt, Phys. Rev. Lett. 1999, 83

[17] "Principles of Instrumental Analysis" Skoog, Holler, and Crouch. Springer Verlag, New York . 1999 pp. 63-65

[18] "Teaching physics with 670-nm diode lasers-experiments with Fabry-Perot cavities" R. A. Boyd, J.L. Bliss, and K.G. Libbrecht, Am. J. Phys., 1996, 64

[19] "Laser Phase and Frequency Stabilization Using an Optical Resonator" R. W. P. Drever, J. L. Hall F. V. Kowalski, J. Hough, G. M. Ford, A. J. Munley, and H. Ward, Applied Physics B, 1983, 31

[20] "Analytical Design of a Confocal Resonator" T. Lofnes, V. Ziemann, and A Ferrari, European Organization for Nuclear Research, 2003, 60

[21] "Notes on the Pound Drever Hall technique" E. Black, Am. J. Phys., 2000, 69 Phys. Rev. A, 2007, 75

[22] "Keeping a Quantum Bit Alive by Optimized π-Pulse Sequences" G. S. Uhrig, Phys. Rev. Lett., 2007, 98

[23] "Optimized Dynamic Decoupling for Time Dependent Hamiltonians" S. Pasini and G.S. Uhrig,2009

[24] "Universality of Uhrig Dynamical Decoupling for Suppressing Qubit Pure Dephasing and Relaxation" W. Yang, and R. B. Liu, Phys. Rev. Lett., 2008, 101

[25] "Near-optimal dynamic decoupling of a qubit" J.R. West, B.H. Fong, and D.A. Lidar, ,2009

[26] "Experimental Uhrig Dynamical Decoupling using Trapped Ions" M. J. Biercuk, et. al., Phys. Rev. A. ,2009, 79